Journal of Controlled Release 368 (2024) 15–23

Contents lists available at ScienceDirect

Journal of Controlled Release

journal homepage: www.elsevier.com/locate/jconrel

Controlling the function of bioactive worm micelles by enzyme-cleavable non-covalent inter-assembly cross-linking

Alina Romanovska, Martin Schmidt, Volker Brandt, Jonas Tophoven, Joerg C. Tiller *

Biomaterials and Polymer Science, Department of Bio- and Chemical Engineering, TU Dortmund, Emil-Figge-Straße 66, 44227 Dortmund, Germany

ARTICLE INFO

Keywords:
Polymer antibtiotic conjugate
Ciprofloxacin
Cross-linked micelles
Lipase-induced release
Poly(2-oxazoline)

ABSTRACT

Drugs that form self-assembled supramolecular structures to be most-active is a promising way of creating new highly specific and active pharmaceuticals. Controlling the activity of bioactive supramolecular structures such as drug-loaded micelles is possible by both core/shell and inter-assembly cross-linking. However, if the flexibility of the assembly is mandatory for the activity cross-linking is not feasible. Thus, such structures cannot be manipulated in their activity.

The present study demonstrates a novel concept to control the activity of not drug-releasing, non-cross-linked bioactive superstructures. This is achieved by formation of nanostructured nanoparticles derived by non-covalent inter-assembly cross-linking of the superstructures. This is shown on the example of amphiphilic diblock-copolymers conjugated with the antibiotic ciprofloxacin (CIP). These polymer-antibiotic conjugates form worm micelles, which greatly activate the conjugated antibiotic without releasing it. Non-covalent inter-assembly cross-linking of these CIP-worm-micelles with amphiphilic triblock copolymers terminated with lipase-cleavable esters leads to nanostructured nanoparticles that resemble cross-linked worm micelles and show an up to 135-fold lower activity than the free worm micelles. The activity of the worm-micelles can be fully recovered by cleaving the end groups of the polymeric cross-linker with lipase.

1. Introduction

A recent branch of modern drug design are constructs with drugs that are embedded into a supramolecular structure. This often self-organized structure, such as spherical [1] or worm micelles [2,3], liposomes [4,5], and polymersomes [6–9] can act as target-selective carrier for a drug or a sensing agent. This way, the active compound is hidden from the immune system and is concentrated at the target side, which minimizes side effects and increases activity or sensitivity. Thereby, the drug can either be attached to the nanostructure by a cleavable bond or can be simply inserted. Besides carrying, directing and protecting a drug, the latter can be released upon external and internal triggers, such as temperature [10], light [11], ultrasound [12], pH or enzymes [13].

Typical rather fragile nanostructures such as polymer micelles [14] that simply act as drug-delivery vehicles can be stabilized by core- or shell-cross-linking, which also allows control of the drug uptake by the cell [15,16]. Numerous self-organized and cross-linked micelles with different shapes [3] and release-profiles caused by either cleavable covalent or non-covalent cross-linking [14] enacted by various stimuli are known [8,17]. This has been applied for many different drug applications, including biocides and antibiotics [18,19]. The activity control of antibiotics is particularly important, because it minimizes the contact time with the immune system reducing the risk of allergic reactions, lowers the bacterial resistance formation, and diminishes cytotoxicity in some cases, e.g. for amphotericin B [20]. Further, the enzymatically triggered release can be induced by bacterial enzymes that are formed by bacterial strains or are at least more present at the infection site, such as hyaluronidase [21] or phosphatase [22].

Also inter-assembly cross-linking of supramolecular structures is known to control drug uptake by cells [23]. However, this is only possible in a reversible manner, if the micelles are already core- or shell-cross-linked. Bioactive superstructures that do not release drugs and act due to folding and unfolding this superstructure, e.g. multivalent enzyme inhibitors [24], will be deactivated by common cross-linking strategies.

Another way of controlling the activity of a drug is to diminish its activity by derivatizing it to create a non-active, non-toxic version, e.g., by blocking functional groups or by binding the drug to a polymer

* Corresponding author.
E-mail address: joerg.tiller@udo.edu (J.C. Tiller).

https://doi.org/10.1016/j.jconrel.2024.02.013
Received 26 November 2023; Received in revised form 6 February 2024; Accepted 9 February 2024
Available online 21 February 2024

[25,26]. Cleaving this group reactivates the drug. In both cases, the drug can be locally activated by cleaving the bond between the drug and the deactivating group, usually chemically or, in more recent work, enzymatically [27–29]. Again, this approach will not work for non-cross-linked supramolecular assemblies as discussed above, because chemical alteration will destroy them. Thus, chemical modification is also not a feasible way of controlling the activity of non-cross-linked self-organized bioactive assemblies.

Here, we present the first example of controlling the activity of a non-cross-linked bioactive superstructure. This has been achieved by the formation of a non-bioactive assembly with telechelic triblock copolymers which gel the worm-like micelles formed by amphiphilic block copolymer ciprofloxacin (CIP) conjugates without destroying their superstructure. This assembly is highly stable in complex media and can be specifically disrupted by enzymatically manipulating the non-active polymer. This fully reactivates the antibacterial activity of the worm-micelles. The presented approach is a concept-driven study and not directed towards a specific infection scenario. The investigated *S. aureus* cells, although clinically relevant, serve as model system.

2. Results and discussion

The present study aims towards a way of non-covalent cross-linking of pharmaceutically active self-assembled supramolecular structures. We chose amphiphilic polymer-antibiotic conjugate (PAC) micelles for employing this strategy. PACs often show a higher antibacterial activity [30], greater efficacy against biofilms [31] and more stability [32]. Particularly, the conjugation of antibiotics, such as penicillin [33] and ciprofloxacin [34], with poly(2-oxazoline)s (POx) has been reported as promising approach to form active PACs with slower bacterial resistance formation and the potential to overcome common resistance mechanisms [35]. More recently, it was demonstrated that the conjugation of CIP with amphiphilic POx-diblock copolymers results in great activation of the antibiotic. Moreover, these amphiphilic PACs form micelles that seem to enter the bacterial cells via their efflux pumps, particularly if they form spherical or worm micelles [36]. The worm micelles carry the antibiotic inside. Intrinsic cross-linking would deactivate them, because the permanently bound drug will not reach its target, the gyrase, anymore. The strategy to control the activity of these micelles was to extrinsically cross-link them into a larger superstructure, because the larger aggregates will not be capable of entering the bacterial cells through their efflux-pump entrances anymore (see Fig. 1). Since the deactivation needs to be reversible and should not interfere with the non-cross-linked superstructure of the amphiphilic PACs, we chose amphiphilic multiblockcopolymers with hydrophobic outer blocks as cross-linker. Such polymers are known to form hydrogels and microgels and we propose that the worm micelles will be incorporated into these gels without destruction of their nanostructure upon nanoprecipitation [37–40]. In order to be able to inverse the structure formation, we chose to introduce the outer hydrophobic blocks as lipase-cleavable units. The cross-linked micelles should be dissolved upon cleaving these groups, releasing the active CIP worm micelles (see Fig. 1). As illustrated in Fig. 1, the concept of this study is based on the presumption that the worm micelle PACs with CIP enter bacterial cells via the pores, e.g. efflux pumps, on the surface. If cross-linked, this worm micelles are to large and inflexible to enter the cells anymore, deactivating them. Cleaving this cross-link will then fully recover their activity. In order to cleave the cross-links, the rather ubiquetous lipase is used as model enzyme to show the feasibility of the new concept.

To find the best suited non-covalent cross-linker for the POx-CIP micelles, a series of POx with two cleavable ester end groups was synthesized. The end groups were varied in hydrophobicity using octanoate and oleate, respectively. The polymer backbone was varyied from hydrophilic poly-2-methyl-oxazoline (PMOx) to amphiphilic triblockcopolymers containing hydrophobic blocks, such as (PHeptOx) or poly-2-phenyl-oxazoline (PPhOx) in the middle. According to their ^{1}H NMR spectra, all polymers show a narrow size distribution and have an end group functionality of >96% in all cases. (for analytical data see supplemetary Table S1).

The resulting copolymers were then codissolved with the worm micelle forming highly active CIP conjugate Me-PMOx$_{15}$-*b*-PHeptOx$_{16}$-EDA-xCIP in ethanol in a 1:1 M ratio (mol/mol) and then added to thorouhgly stirred water. A successful formation of larger aggregates is initially judged by a visible precipitation. As seen in Table 1, the telechelic homopolymers did not aggregate with the worm micelles, while all end-group-esterified triblockcopolymers rendered the mixture

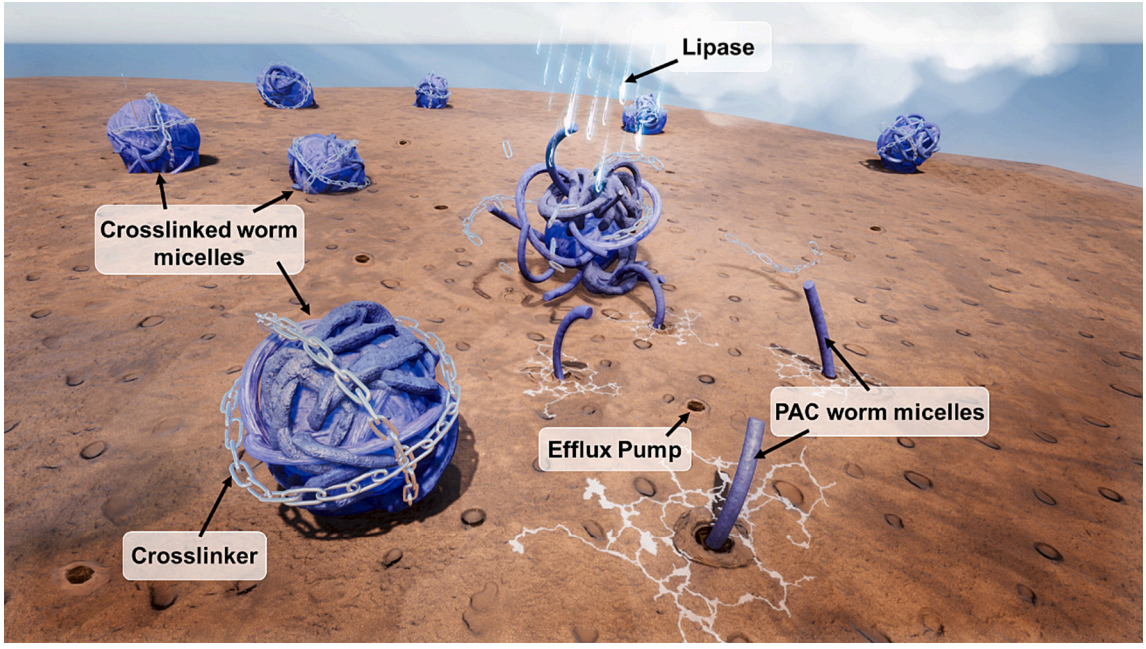

Fig. 1. Illustration of the general concept of controlling the activity of cross-linked, antibacterial worm micelles based on CIP-based antibiotic polymer conjugates (PAC) on a bacterial surface. The worm micelles are inactive in its cross-linked state and can be released and activated by the cross-linker cleaving enzyme lipase. The activated worm micelles enter the bacterial cell via their efflux pumps and kill the cell from within.

Table 1
Yields of isolated aggregates after nanoprecipitation, contents of the CIP conjugate within the aggregates, MIC-values and On-Off-Factors as MIC (CIP conjugate in aggregate)/MIC (free CIP conjugate). The MIC values in Table 1 are expressed as mean ± SD (n = 3–4).

Polymer	Isolated Yield [%]	CIPconjugate [mol%][a]	$MIC_{S.a.}$ [μg·mL^{-1}]	On-Off-$Factor_{S.a.}$
C_8-$PMOx_{36}$-C_8	–			
C_{18}-$PMOx_{36}$-C_{18}	–			
C_8-$PMOx_{13}$-*b*-$PHeptOx_{26}$-*b*-$PMOx_{13}$-C_8	30	n.d.[b]	7 ± 2	1–2
C_8-$PMOx_5$-*b*-$PPhOx_9$-*b*-$PMOx_5$-C_8	10	39	6 ± 2	1–2
C_8-$PMOx_{10}$-*b*-$PPhOx_{10}$-*b*-$PMOx_{10}$-C_8	15	36.7	16 ± 3	5
C_8-$PMOx_{17}$-*b*-$PPhOx_{20}$-*b*-$PMOx_{17}$-C_8	55	25.9	102 ± 19	14
C_8-$PMOx_{10}$-*b*-$PPhOx_{20}$-*b*-$PMOx_{10}$-C_8	63	37.5	527 ± 25	135
C_8-$PMOx_{10}$-*b*-$PPhOx_{40}$-*b*-$PMOx_{10}$-C_8	62	39	88 ± 13	24

[a] Mol% of Me-$PMOx_{15}$-*b*-$PHeptOx_{16}$-EDA-xCIP in the isolated aggregate determined by ^{1}H NMR spectroscopy (cf. spectra shown in Figs. S4–8 in the supplementary information and see determination in the experimental part).
[b] Not detectable from the respective ^{1}H NMR spectrum.

cloudy. The isolated water-insoluble solids were analyzed by TEM. As seen in Fig. 2a, the end-group-esterified triblockcopolymer C_8-$PMOx_{10}$-*b*-$PPhOx_{40}$-*b*-$PMOx_{10}$-C_8 alone precipitates as sphere without recognizable structure.

The same is true for all other end-group-esterified triblockcopolymers (see supplements, Fig. S11). The nanoprecipitation of the CIP conjugate results in rod or worm micelles (see Fig. 2b). Addition of triblockcopolymer with a PHeptOx as middle block to the CIP conjugate leads to particles without ordered structure surrounded by somehow bend elongated worm micelles (see Figs. 2c). This structural change of the coprecipitate suggests that the triblockcopolymer and the diblockcopolymer of the CIP conjugate somewhat mix and form a new structure as known from numerous other studies on the structures derived by mixed blockcopolymers [41–43]. The aggregates with the triblockcopolymers that have PPhOx as middle block seem the contain the unchanged worm micelles in all cases, indicating that the different polymers do not mix and thus, the triblockcopolymer can act as cross-linker only (see Figs. 2d-i). The TEM images in Fig. 2 d-i also show that the way of cross-linking depends on the structure of the coprecipitated triblockcopolymer. Short polymers such as C_8-$PMOx_5$-*b*-$PPhOx_9$-*b*-$PMOx_5$-C_8 and C_8-$PMOx_{10}$-*b*-$PPhOx_{10}$-*b*-$PMOx_{10}$-C_8 appear to elongate the CIP worm micelles into loose, fiber-like structures (see Figs. 2d and e). Increasing the length of the triblockcopolymers seems to increase the number of cross-links, which leads to a more dense structure of the precipitate. For example, the triblockcopolymer C_8-$PMOx_{17}$-*b*-$PPhOx_{20}$-*b*-$PMOx_{17}$-C_8 forms a fiberous networks with the CIP conjugate that resembles loosely cross-linked worm micelles. Also the hydrophilic/hydrophobic balance of the triblockcopolymers influences the structure afforded by nanocoprecipitation with the CIP-conjugate. The triblockcopolymers with a longer hydrophobic middle block C_8-$PMOx_{10}$-*b*-$PPhOx_{20}$-*b*-$PMOx_{10}$-C_8 and C_8-$PMOx_{10}$-*b*-$PPhOx_{40}$-*b*-$PMOx_{10}$-C_8 afford nanostructured particles, which resemble densly cross-linked worm micelles. The structural motive of the wool-cluster-like aggregates with C_8-$PMOx_{10}$-*b*-$PPhOx_{20}$-*b*-$PMOx_{10}$-C_8 and Me-$PMOx_{15}$-*b*-$PHeptOx_{16}$-EDA-xCIP seen in the TEM image was confirmed by SAXS measurement of the dried and swollen aggregates (Fig. S12). The dried aggregates show a strong correlation peak with a d value of 11.3 nm, which can be translated as distance between the micelles. Swelling the aggregates in water results in a stronger correlation peak, which is shifted to 12.7 nm. It confirms that the swollen aggregates have most likely the same ordered structure as in dried form, which indicates the high stability of this supramolecular structure. According to the SAXS measurement, a water uptake of 42% can be estimated for the cross-linked worm micelles. The proposed association mechanism of the cross-linked micelles based on the structures found in the TEM images is shown in Fig. 3. Thereby, only the end-groups of the triblockcopolymers act as cross-linking groups for the worm micelles, while the PPhOx middle block does not interact with them. This is why the micelles keep their shape even in cross-linked state.

The composition of the cross-linked micelles was determined via the [1]HNMR spectra of the precipitates dissolved in chloroform (Table 1, Fig. S4–8). The detailed description of this calculation is provided in the experimental part (nanoprecipitation method). According to this, the triblockcopolymers and the CIP-conjugate do not precipitate in the same ratio (1:1 mol/mol) as applied in the stock solution. The precipitates contain only 27 to 39 mol% of the CIP conjugate (see Table 1). This is somewhat expected, because the large spheres formed by the triblock copolymers will be easily centrifuged off, while the worm micelles originating from the CIP conjugate cannot be isolated this way and therefore not fully cross-linked worm micelles will be lost upon purification. In order to investigate if the composition and the yield of the cross-linked micelles can be influenced by varying the composition in the stock solution, $PMOx_{10}$-*b*-$PPhOx_{20}$-*b*-$PMOx_{10}$-C_8 and Me-$PMOx_{15}$-*b*-$PHeptOx_{16}$-EDA-xCIP were nanoprecipitated with an ethanolic solution containing the polymers in a 2:1 and a 1:2 M ratio, respectively (cf. ^{1}H NMR spectra in Figs. S9–10). The first experiment resulted in a precipitate that contains only 29 mol% of the CIP conjugate. This drop from 37.5 mol% for the precipitate derived from the solution with 1:1 mol triblock copolymer/mol CIP conjugate ratio can be explained by the high excess of the triblock copolymer. Rather surprisingly, the precipitate from the solution with 1:2 mol triblock copolymer/mol CIP conjugate ratio was found to contain 39 mol% of the CIP-conjugate, which is close to that obtained by the 1:1 ratio.

To explore, if the formed aggregates truly deactivate the CIP worm micelles, the minimal inhibitory concentration (MIC) against the bacterium *Staphylococcus aureus (S. aureus)* was determined by dispersing the cross-linked micelles in a bacterial growth medium, inoculating it with the bacterial cells (10^5 cells per mL), incubating overnight at 37 °C, and photometrically detecting the lowest concentration, which prevents the growth of the bacterial cells to at least 99%. As seen in Fig. 4, the aggregate of Me-$PMOx_{15}$-*b*-$PHeptOx_{16}$-EDA-xCIP with C_8-$PMOx_{10}$-*b*-$PPhOx_{20}$-*b*-$PMOx_{10}$-C_8 shows the highest deactivation of 135 compared to the free conjugate. The deactivation of the CIP-conjugate by the triblock copolymers with a lower PPhOx content or a shorter chain length is less pronounced, which is most likely due to the lower stability of the aggregates. The same is true for the triblock copolymer C_8-$PMOx_{13}$-*b*-$PHeptOx_{26}$-*b*-$PMOx_{13}$-C_8. This can be explained by the possibility of the two polymers to mix and thus form mixed micelles, which are not forming a stable aggregate and are thus available at the surface of the bacterial cells. The stability of the conjugates was tested in the highly complex bacterial growth medium, which contains several buffer salts, peptides and proteins. To this end, a dilution series of the aggregates Me-$PMOx_{15}$-b-$PHeptOx_{16}$-EDA-xCIP with C_8-$PMOx_{10}$-b-$PPhOx_{20}$-b-$PMOx_{10}$-C_8 in the bacterial growth medium was prepared for the MIC-test, left for 12 h at 37 °C, and was then inoculated with *S. aureus* cells. The resulting MIC was found to be the same as that obtained by directly inoculating the solution with the bacterial cells, clearly indicating that the suspended aggregates are stable in this complex mixture.

Next, it was explored, if the cross-linking concept only works for worm micelles. A similar CIP-conjugate - Me-$PMOx_{22}$-*b*-$PHeptOx_8$-EDA-xCIP - forms sperical micelles due to the molar ratio of PHeptOx/PMOx (see Fig. 5a). The MIC value of this conjugate against *S. aureus* is 0.12 μmol·L^{-1} (0.4 μg·mL^{-1}). This conjugate was nanoprecipitated with C_8-

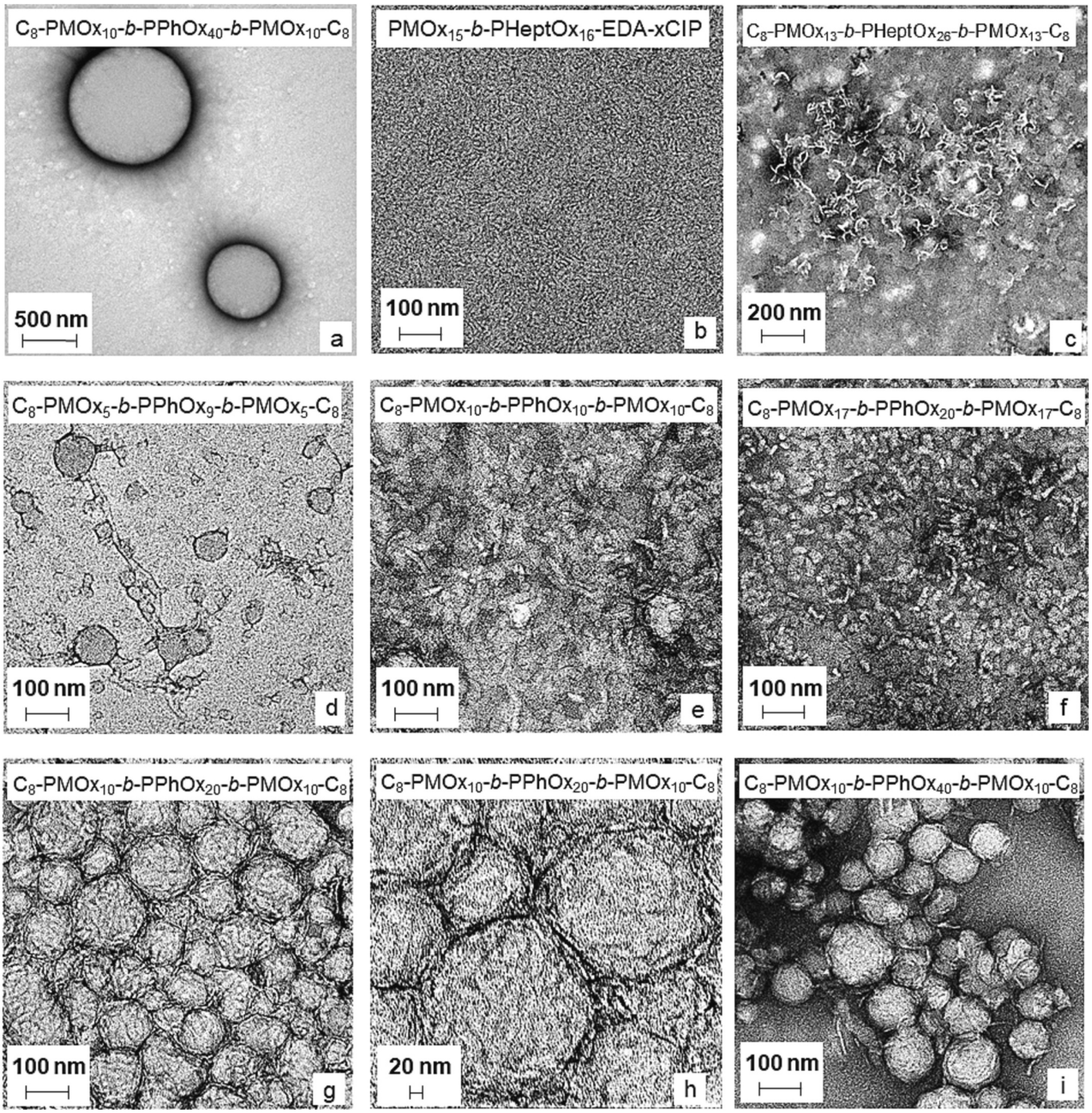

Fig. 2. TEM measurements of structures formed by nanoprecipitation from ethanol to water. a: C_8-$PMOx_{10}$-*b*-$PPhOx_{40}$-*b*-$PMOx_{10}$-C_8, b: Me-$PMOx_{15}$-*b*-$PHeptOx_{16}$-EDA-xCIP. Precipitates with Me-$PMOx_{15}$-*b*-$PHeptOx_{16}$-EDA-xCIP: c: C_8-$PMOx_{13}$-*b*-$HeptOx_{26}$-*b*-$PMOx_{13}$-C_8, d: C_8-$PMOx_5$-*b*-$PPhOx_9$-*b*-$PMOx_5$-C_8, e: C_8-$PMOx_{10}$-*b*-$PPhOx_{10}$-*b*-$PMOx_{10}$-C_8, f: C_8-$PMOx_{17}$-*b*-$PPhOx_{20}$-*b*-$PMOx_{17}$-C_8, g: C_8-$PMOx_{10}$-*b*-$PPhOx_{20}$-*b*-$PMOx_{10}$-C_8, h: C_8-$PMOx_{10}$-*b*-$PPhOx_{40}$-*b*-$PMOx_{10}$-C_8, i: C_8-$PMOx_{10}$-*b*-$PPhOx_{20}$-*b*-$PMOx_{10}$-C_8. Precipitation was performed from an ethanolic solution of the polymers and polymer mixtures in an excess of water. Samples were stained with Ruthenium chloride.

$PMOx_{10}$-*b*-$PPhOx_{20}$-*b*-$PMOx_{10}$-C_8 from an ethanolic solution containing a 1:1 (mol/mol) ratio of the two polymers. As seen in Fig. 5b, the formed aggregate is obviously composed of cross-linked spherical micelles, which shows that the concept works for spherical micelles as well and also that the triblockcopolymer only acts as cross-linker and does not influence the structure of the CIP-conjugates. The aggregate also shows a diminished antibacterial activity against *S. aureus* of the CIP-conjugate by a factor of 42.

The concept is based on the idea that the structure of the aggregates is majorly stabilized by the hydrophobic end groups of the cross-linking triblockcopolymer. Thus cleaving these groups might reverse the cross-linking process. To investigate this, the cleavage of the ester functions from the triblockcopolymers was investigated first. The esterified triblocopolymers were nanoprecipitated in water, isolated by centrifugation and suspended in aqueous NaOH (0.03 M). The cloudy suspension was stirred at room temperature and cleared after 2 h in all cases, except for C_8-$PMOx_{10}$-*b*-$PPhOx_{40}$-*b*-$PMOx_{10}$-C_8, which did not turn clear even after 7d. According to the ^{1}H NMR the isolated polymers showed no

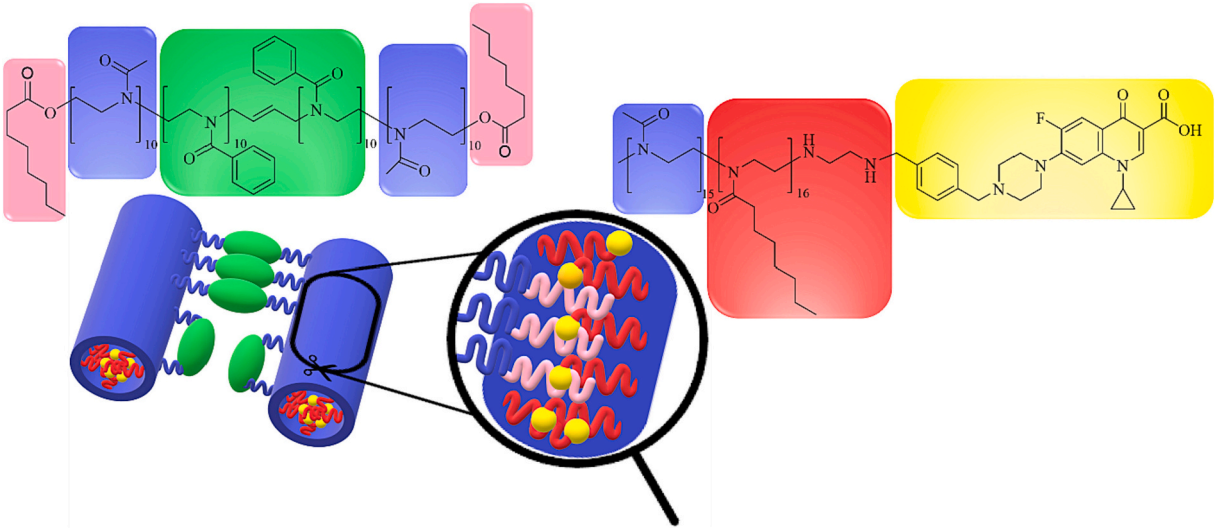

Fig. 3. Schematic representation of the macromolecular crosslinking between triblock copolymers and a worm micelle forming PAC. Interaction between the triblock copolymer C_8-$PMOx_{10}$-b-$PPhOx_{20}$-*b*-$PMOx_{10}$-C_8 and Me-$PMOx_{15}$-*b*-$PHeptOx_{16}$-EDA-xCIP. The magnification illustrates how only the hydrophobic alkyl chains of both polymers overlap in the core of the structure. We presume that cleaving the (pink) end groups will diminish all interactions between the polymers and "free" the worm micelles. (For interpretation of the references to colour in this figure legend, the reader is referred to the web version of this article.)

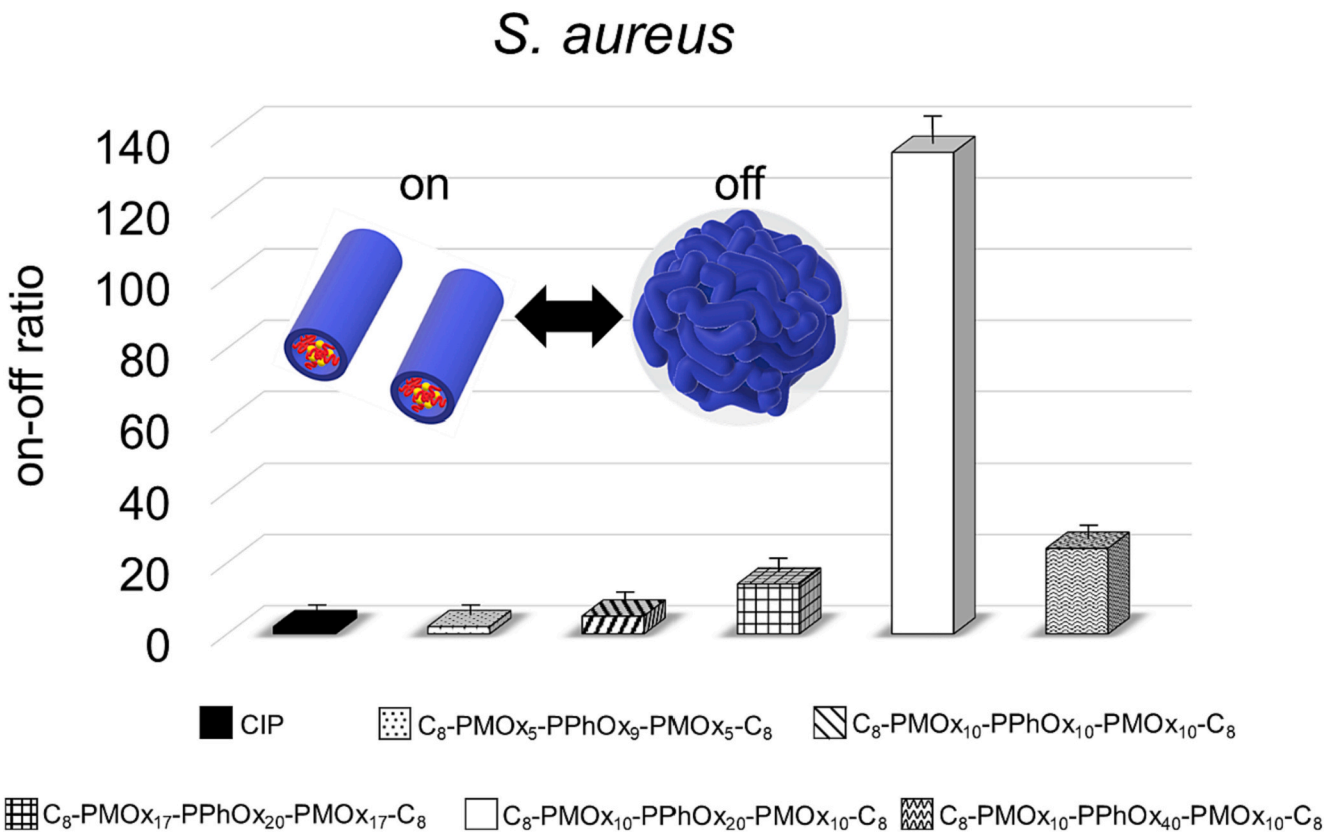

Fig. 4. On-off ratio of the cross-linked conjugate Me-$PMOx_{15}$-*b*-$PHeptOx_{16}$-EDA-xCIP with different triblock copolymers. C_8-$PMOx_5$-*b*-$PPhOx_{10}$-*b*-$PMOx_5$-C_8 (dotted), C_8-$PMOx_{10}$-*b*-$PPhOx_{10}$-*b*-$PMOx_{10}$-C_8 (striped), C_8-$PMOx_{17}$-*b*-$PPhOx_{20}$-*b*-$PMOx_{17}$-C_8 (checkered), C_8-$PMOx_{10}$-*b*-$PPhOx_{20}$-*b*-$PMOx_{10}$-C_8 (white) and C_8-$PMOx_{10}$-*b*-$PPhOx_{40}$-*b*-$PMOx_{10}$-C_8 (waved) and the MIC-values of CIP (black). Values in Fig. 4 are expressed as mean ± SD (n = 3–4). The on-off ratio is defined as MIC value of the CIP conjugate in the aggregate divided by MIC of the free CIP conjugate. The MIC of the free CIP conjugate against *S. aureus* is 0.4 μmol·L^{-1} (1.5 μg·mL^{-1}) determined with the same protocol used of all tests given in the experimental part. All other polymers with and without octanoate end groups show no antibacterial activity against *S. aureus*.(no activity measured up to 500 μg·mL^{-1}).

ester groups after reaching this clearing point (Fig. S2). The same protocol was applied for the cross-linked micelles. In case of the cross-linked system, the hydrolysis is slower and the clearing point is reached after 8–12 h. The solution was then neutralized with hydrochloric acid, dried under air flow and subjected to the MIC-test against *S. aureus*. It was found that the disruption of the aggregates caused by cleaving the ester

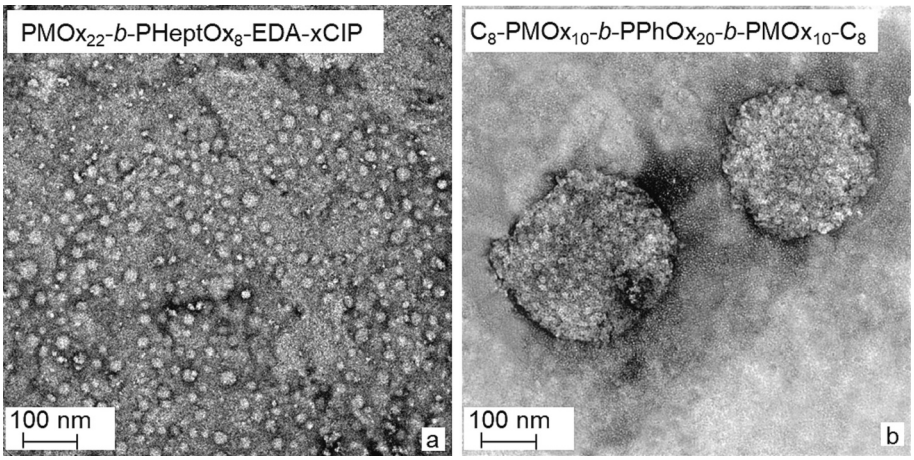

Fig. 5. TEM images of spherical micelles and the crosslinking of these with a triblock copolymer. a: spherical micelles consisting of Me-PMOx$_{22}$-*b*-PHeptOx$_8$-EDA-xCIP formed by nanoprecipitation and b: the aggregates consisting of triblock copolymer C$_8$-PMOx$_{10}$-*b*-PPhOx$_{20}$-*b*-PMOx$_{10}$-C$_8$ and CIP conjugate Me-PMOx$_{22}$-*b*-PHeptOx$_8$-EDA-xCIP.

end groups of the triblocopolymer results in full activation of the CIP conjugate. As shown in the TEM image in Fig. 6b, the hydrolysis of the coprecipitates results in coexisting spherical micelles formed by the triblockcopolymer without ester end groups (Fig. 6a) and the free worm micelles formed by the CIP conjugate.

Dynamic light scattering of the solutions confirmed the full disruption of the aggregates after reaching the clearing point (see Fig. S13). It was now explored, if this result can also be achieved when catalyzing the ester cleavage by the enzyme lipase. After adding lipase in an activity typical for human blood at neutral pH to the cross-linked micelle suspensions, it took at least 18 h to reach the clearing point. Again, the full antibacterial activity of the respective CIP conjugate against *S. aureus* was found in the cleared solutions. In order to get insights into the kinetics of this process, the CIP conjugate cross-linked by C$_8$-PMOx$_{10}$-*b*-PPhOx$_{20}$-*b*-PMOx$_{10}$-C$_8$ was treated with the same amount of lipase for different periods of time and the mixture was then subjected to the MIC-test against *S. aureus*. When applied to the MIC-test, the conjugate and also the lipase are highly diluted. Thus we presume that no significant further ester cleavage will occur during the determination of the MIC. The obtained MIC$_{S.aureus}$ values show that the CIP conjugate activation occurs very quickly at the beginning of the reaction. The MIC$_{S.aureus}$ after 2 h is 12 μg·mL^{-1} indicating that already to 33% of the CIP conjugate is released. The MIC$_{S.aureus}$ increases to 4 μg·mL^{-1} after 18 h. This value is that of the free CIP conjugate in such a mixture, indicating that practically all worm micelles are released after this time. Thus, a typical lipase concentration in the human body might be suitable to fully re-activate the worm micelles from their cross-linked aggregates.

3. Conclusion

It could be demonstrated in this study that a bioactive, self-organized supramolecular structure can be controlled in its bioactivity by non-covalent cross-linking with suited amphiphilic multiblockcopolmers via nanoprecipitation. This method is efficient and does not destroy the supramolecular structure. The cross-links can be cleaved with lipase, which leads to releasing the active superstructure. This is clearly

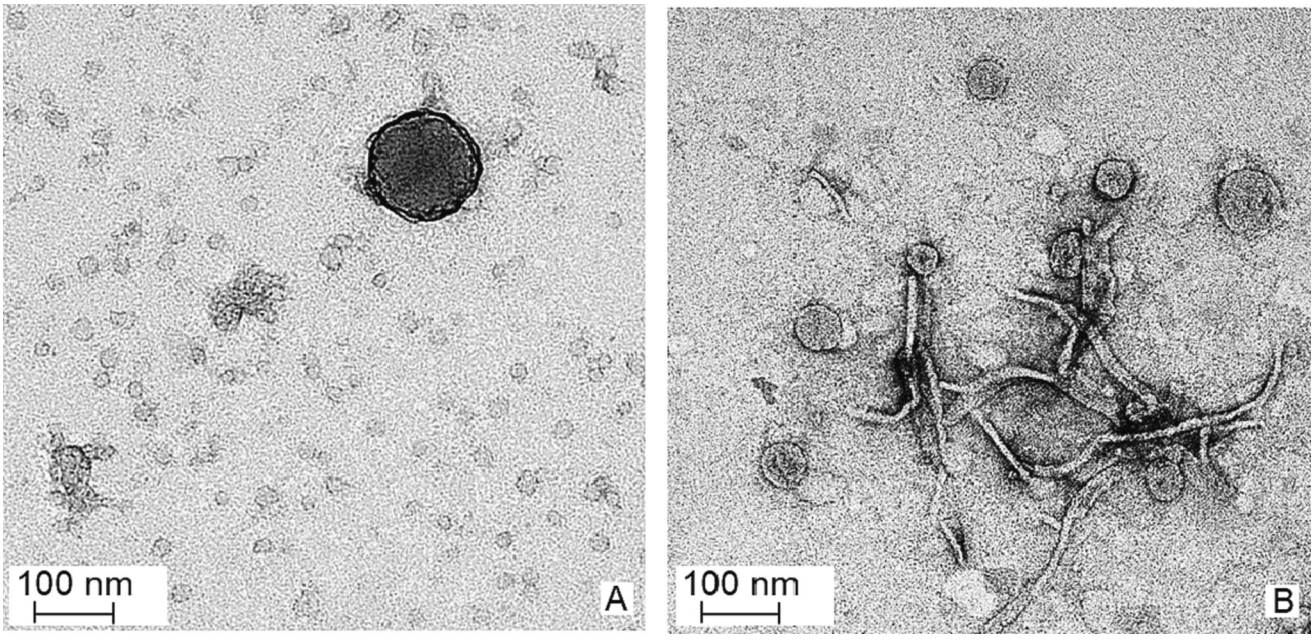

Fig. 6. TEM measurements of the fully NaOH-hydrolysed nanoprecipitate of the triblock copolymer C$_8$-PMOx$_{10}$-*b*-PPhOx$_{20}$-*b*-PMOx$_{10}$-C$_8$ (a) of the fully NaOH-hydrolysed triblock copolymer C$_8$-PMOx$_{10}$-*b*-PPhOx$_{20}$-*b*-PMOx$_{10}$-C$_8$ nanoprecipitated with Me-PMOx$_{15}$-*b*-PHeptOx$_{16}$-EDA-xCIP in a 1:1 ratio (b).

different from other enzyme-induced biocide and antibiotic releasing systems, which release low molecular weight compounds, peptides or polymers, but not superstructures, from covalently or non-covalently nanoparticles or gels [13]. The cross-linking multiblockcopolymers need to be perfectly balanced in their composition and structure to be effective. The presented concept will be transferrred to other drugs, such as chemostatica or specific, complex enzyme inhibitors in future work.

4. Materials and methods

Materials. The reactions, purifications and polymerisations were carried out under an inert atmosphere. Acetonitrile (Fisher Scientific) was distilled from diphosphorus pentoxide (VWR), then from potassium carbonate (VWR), and stored over 3 Å molecular sieves. The water content was determined by Karl Fischer titration (<0.5 ppm). The initiator *trans*-1,4-dibromo-2-butene (DBB) was purchased from Acros Organics and recrystallized from dry chloroform two times, dried in atmosphere at 25 °C, and stored under argon atmosphere. 2-Methyl-2-oxazoline (MOx, ACROS) and 2-phenyl-2-oxazoline (PhOx, Sigma-Aldrich) were distilled under reduced pressure from calcium hydride (ACROS). 2-Heptyl-2-oxazoline (HeptOx) was synthesized according to literature [44]. Lipase from *Aspergillus niger* (187 U/g) was purchased from Sigma-Aldrich. The bacterial strain *Staphylococcus aureus* (gram-positive, ATCC 25323) was provided by the German Resource Center for Biological Material (DSMZ).

Measurements. ^{1}H NMR spectra were recorded in deuterated solvents ($CDCl_3$) using FT-appliances of Varian type Inova 500 (500 MHz) or FT-appliances of Bruker, types DPX-300 (300 MHz), DRX-400 (400 MHz), DRX-500 (500 MHz). The residual protons of the not fully deuterated solvents served as an internal standard.

Transmission electron micrographs were acquired on an Talos F200X microscope operating at an accelerating voltage of 200 kV. The polymer samples were dissolved in distilled water (1 wt%) and dropped on carbon-coated copper grids allowing the solvent to evaporate. A staining solution was prepared as follows. 0.2 g of ruthenium chloride hydrate and 10 mL (5 wt%) sodium hypochlorite were dissolved in 100 mL distilled deionized water. The grids with the polymeric sample were incubated with three droplets of staining solution. After 20 min, the samples were analyzed by transmission electron microscopy (TEM).

SAXS measurements were performed on the Bruker NANOSTAR instrument using a VANTEC-2000 detector and an IμS microfocus source (Incoatec GmbH) with a Cu anode (wavelength $\lambda = 0.154$ nm) and integrated Montel optics. Calibration was performed with a silver behenate standard and the distance between the samples and the detector was 107 cm. All measurements were performed at room temperature and under vacuum. Samples were filled both dry and swollen into fused silica capillaries, which were sealed at both ends. The SAXS measurements were each recorded over one hour, followed by azimuthal integration to obtain the scattered intensities as a function of the magnitude of the scattering vector $q = 4\pi\sin(\theta)/\lambda$ (2θ = diffraction angle).

The SAXS measurements were needed to determine the swelling properties of the polymer particles. The polymer particles were measured on the SAXS in the dry state and in the swollen state. The water content of the swollen particles was calculated according to Wilhelm et al. [45]

Dynamic light scattering (DLS) measurements were performed on a Malvern Zetasizer Nano S (ZEN 1600) in water at 25 °C with polymer concentrations varying from 0.5 to 10 wt%. The distribution curve was calculated with a CONTIN fit for random distribution.

Nanoprecipitation method. 9.5 mg of the polymer-antibiotic conjugate (PAC) and the equimolar amount of cross-linker polymer were dissolved in 0.4 mL ethanol. The method was also performed with the only the cross-linker polymers and the PAC, respectively. The whole ethanolic solution was added to 2.4 mL of very fast stirring deionized water contained in a snap cap within 10 s using a syringe and the mixture was stirred for 2 h. The precipitate was isolated upon centrifugation (HERMLE Z300) at 6000 rpm for 10 min and the solid was washed with distilled water three times. The solid was then dried in atmosphere (Isolated yield from the nanoprecipitation of Me-PMOx$_{15}$-*b*-PHeptOx$_{16}$-EDA-xCIP and C$_8$-PMOx$_{10}$-*b*-PPhOx$_{20}$-*b*-PMOx$_{10}$-C$_8$: 63%, all yields are given in Table 1). The composition of the nanoprecipitates was determined from the ^{1}H NMR spectra shown in the supplementary Figs. S4-S8. To this end the integrals of the two starter protons of the triblockcopolymers at 5.35 ppm ($A_1 = 2$, reference) that of all CH_3 groups in both polymers (end groups of the triblockcopolymer and heptyl side chain of the CIP conjugate) at 0.88 ppm (A_2) were used. The latter signal is then composed of 6 protons for 1 mol of the triblockcopolymer and 48·x for x mol of the CIP conjugate. The molar content of the CIP conjugate was calculated as follows: mol% (CIP conjugate) = x/(1 + x)·100 with x = (A2–6)/48.

End group hydrolysis of the ABA triblock copolymers. 10 mg of the cross-linked PAC obtained be nanoprecipitation was suspended in 2 mL of aqueous 0.03 M NaOH and stirred at 37 °C. The hydrolysis success is evaluated optically or by means of the DLS measurement. After reaching the clearing point, the solution was neutralized with 0.1 M hydrochloric acid and subjected to the MIC-test. The same experiment was performed with and aqueous lipase solution (2 mg·mL^{-1}). Here, the solution was subjected to the MIC-test without neutralizing.

Synthesis of 2-R-2-oxazolines, 7-(4-(4-(Chloromethyl)benzyl)piperazin-1-yl)-1-cyclopropyl-6-fluoro-4-oxo-1,4 dihydroquino-line-3-carboxylic acid (xCIP-Spacer), General Procedure for the Polymerization of amphiphilic Polymers and General Procedure of xCIP-Linking. The syntheses were carried out according to literature [34,46].

Preparation of Poly(2-methyloxazoline)-block-poly(2-phenyloxazoline)-block-poly(2-methyloxazoline) ABA-Triblock Copolymers. Under argon, a mixture of 316.5 mg (1.48 mmol, 1 equiv) of DBB and PhOx (4.4 g, 29.6 mmol, 20 equiv) or HeptOx (5 g, 29.6 mmol, 20 equiv) was dissolved in 15 mL of dry MeCN. The mixture was heated at 160 °C for 5 h (PPhOx) or at 130 °C for 2 h (PHeptOx) in a microwave reactor. If a homopolymer is required, the termination of the polymer is initiated at this point, otherwise the further instructions for the second monomer and the subsequent termination follow. After cooling to 50 °C, MOx (2.44 g, 28.77 mmol, 20 equiv) was added and then the mixture was heated at 100 °C for 2 h. The living polymer solution was terminated with 0.47 mL (426 mg, 2.96 mmol, 2 equiv.) of caprylic acid or 0.94 mL (836.1 mg, 2.96 mmol, 2 equiv.) oleic acid and 0.56 mL (421 mg, 3.26 mmol, 2.2 equiv) *N,N*-diisopropylethylamine and heated at 50 °C for 72 h. Finally, the mixture was purified by dialysis in methanol for 4 h and the purified polymers were obtained in yields of 90–93%.

C$_8$-PMOx$_{10}$-*b*-PEPOx$_{10}$-*b*-PMOx$_{10}$-C$_8$ ^{1}H NMR (400 MHz, chloroform-*d*) δ = ppm 0.81 (s, 3H) 1.21 (br. s., 8H) 1.48–1.59 (m, 2H) 1.74–2.14 (m, 20H) 2.16–2.29 (m, 2H) 2.63–3.91 (m, 38H) 4.04–4.23 (m, 4H) 5.07–5.54 (m, 2H) 6.71–7.81 (m, 5H).

Minimal Inhibitory Concentration (MIC). The investigation of the antimicrobial activity of samples was carried out according a varied protocol from the literature [47]. A stock solution of *S. aureus* (Gram-positive, strain ATCC 25323) was prepared from a stock pellet (from DSMZ, see the Materials section) in a standard I nutrient broth (NB, Merck, 50 mL) at pH 7.38. After incubation at 37 °C for 12 h, the sample was diluted with NB to 10^9 cells per mL. A sample of the CIP conjugate or the co-nanoprecipitated CIP conjugate and triblockcopolymer (20.0 mg) was dissolved or suspended in NB (4.00 mL), and a dilution series was prepared with halved concentrations in every following sample. Every sample was inoculated with the bacterial solution (20 μL, 10^9 cells per mL) to afford a concentration of 10^7 cells per mL and incubated at 37 °C for another 12 h. Then, 100 μL of a 2,3,5-triphenyltetrazolium chloride (TCC, Sigma)-solution in water (1 mg mL^{-1}) was added. After further 3 h of incubation, the samples with the highest concentration that showed no coloration were considered as MIC value. Control measurement with NB inoculated with different concentrations of *S. aureus* cells incubated with TCC showed that a cell concentration of 10^6 cells per mL already

results in a clearly visible red coloration. Thus, the reduction of the *S. aureus* cells at the MIC value is at least 99%.

Statistical Analysis. All values were expressed as mean ± standard deviation (SD). The results were analyzed statistically using a one-way ANOVA, followed by a Tukey post-hoc test. In all cases, the significance was set at $p \leq 0.05$. Statistical analysis was carried out using OriginPro 2020b Software.

Author contributions

J.C.T. and A.R. designed the study, interpreted the results and wrote the manuscript. A.R. and J.T. carried out all synthesis of the di- and triblock copolymers, prepared the TEM images and MIC tests. M.S. and A.R. performed the lipase tests.

CRediT authorship contribution statement

Alina Romanovska: Writing – original draft, Methodology, Investigation, Data curation. **Martin Schmidt:** Writing – original draft, Visualization, Investigation, Conceptualization. **Volker Brandt:** Investigation. **Jonas Tophoven:** Investigation. **Joerg C. Tiller:** Writing – review & editing, Validation, Supervision, Conceptualization.

Data availability

Data will be made available on request.

Acknowledgement

All polymers were synthesized using CEM Discover microwaves, which were kindly provided by CEM for ungraduated student education. We thank Dr. Wolf Hiller and his team from the department of chemistry for recording the NMR spectra at the TU Dortmund. The TEM was in part financed by the DFG in grant INST 212/423-1 FUGG.

Appendix A. Supplementary data

Supplementary data to this article can be found online at https://doi.org/10.1016/j.jconrel.2024.02.013.

References

[1] B. Ghosh, S. Biswas, Polymeric micelles in cancer therapy: state of the art, J. Control. Release 332 (2021) 127–147, https://doi.org/10.1016/j.jconrel.2021.02.016.
[2] P. Lagarrigue, F. Moncalvo, F. Cellesi, Non-spherical polymeric nanocarriers for therapeutics: the effect of shape on biological systems and drug delivery properties, Pharmaceutics 15 (2023) 32, https://doi.org/10.3390/pharmaceutics15010032.
[3] K. Klinker, et al., Secondary-structure-driven self-assembly of reactive polypept(o)ides: controlling size, shape, and function of core cross-linked nanostructures, Angew. Chem. Int. Ed. 56 (2017) 9608–9613, https://doi.org/10.1002/anie.201702624.
[4] D.E. Large, R.G. Abdelmessih, E.A. Fink, D.T. Auguste, Liposome composition in drug delivery design, synthesis, characterization, and clinical application, Adv. Drug Deliv. Rev. 176 (2021) 113851, https://doi.org/10.1016/j.addr.2021.113851.
[5] M. Abri Aghdam, et al., Recent advances on thermosensitive and pH-sensitive liposomes employed in controlled release, J. Control. Release 315 (2019) 1–22, https://doi.org/10.1016/j.jconrel.2019.09.018.
[6] M.G. Gouveia, et al., Polymersome-based protein drug delivery – quo vadis? Chem. Soc. Rev. 52 (2023) 728–778, https://doi.org/10.1039/D2CS00106C.
[7] M. Baghbanbashi, A. Kakkar, Polymersomes: soft nanoparticles from Miktoarm stars for applications in drug delivery, Mol. Pharm. 19 (2022) 1687–1703, https://doi.org/10.1021/acs.molpharmaceut.1c00928.
[8] K. Kuperkar, D. Patel, L.I. Atanase, P. Bahadur, Amphiphilic block copolymers: their structures, and self-assembly to polymeric micelles and polymersomes as drug delivery vehicles, Polymers 14 (2022) 4702, https://doi.org/10.3390/polym14214702.
[9] Y. Zhu, S. Cao, M. Huo, J.C.M. van Hest, H. Che, Recent advances in permeable polymersomes: fabrication, responsiveness, and applications, Chem. Sci. 14 (2023) 7411–7437, https://doi.org/10.1039/D3SC01707A.
[10] M. Ghezzi, et al., Polymeric micelles in drug delivery: an insight of the techniques for their characterization and assessment in biorelevant conditions, J. Control. Release 332 (2021) 312–336, https://doi.org/10.1016/j.jconrel.2021.02.031.
[11] J. Zhu, T. Guo, Z. Wang, Y. Zhao, Triggered azobenzene-based prodrugs and drug delivery systems, J. Control. Release 345 (2022) 475–493, https://doi.org/10.1016/j.jconrel.2022.03.041.
[12] F. Moradi Kashkooli, A. Jakhmola, T.K. Hornsby, J. Tavakkoli, M.C. Kolios, Ultrasound-mediated nano drug delivery for treating cancer: Fundamental physics to future directions, J. Control. Release 355 (2023) 552–578, https://doi.org/10.1016/j.jconrel.2023.02.009.
[13] Q. Zhou, et al., Enzyme-triggered smart antimicrobial drug release systems against bacterial infections, J. Control. Release 352 (2022) 507–526, https://doi.org/10.1016/j.jconrel.2022.10.038.
[14] M. Lin, Y. Dai, F. Xia, X. Zhang, Advances in non-covalent crosslinked polymer micelles for biomedical applications, Mater. Sci. Eng. C 119 (2021) 111626, https://doi.org/10.1016/j.msec.2020.111626.
[15] Y. Kim, M.H. Pourgholami, D.L. Morris, M.H. Stenzel, Effect of cross-linking on the performance of micelles as drug delivery carriers: a cell uptake study, Biomacromolecules 13 (2012) 814–825, https://doi.org/10.1021/bm201730p.
[16] M. Talelli, et al., Core-crosslinked polymeric micelles: principles, preparation, biomedical applications and clinical translation, Nano Today 10 (2015) 93–117, https://doi.org/10.1016/j.nantod.2015.01.005.
[17] J. Li, K. Kataoka, Chemo-physical strategies to advance the in vivo functionality of targeted nanomedicine: the next generation, J. Am. Chem. Soc. 143 (2021) 538–559, https://doi.org/10.1021/jacs.0c09029.
[18] C.H. Ho, E.K. Odermatt, I. Berndt, J.C. Tiller, Long-term active antimicrobial coatings for surgical sutures based on silver nanoparticles and hyperbranched polylysine, J. Biomater. Sci. Polym. Ed. 24 (2013) 1589–1600, https://doi.org/10.1080/09205063.2013.782803.
[19] S. Tian, H.C. van der Mei, Y. Ren, H.J. Busscher, L. Shi, Co-delivery of an amyloid-disassembling polyphenol cross-linked in a micellar Shell with core-loaded antibiotics for balanced biofilm dispersal and killing, Adv. Funct. Mater. 32 (2022) 2209185, https://doi.org/10.1002/adfm.202209185.
[20] R. Fernández-García, et al., Self-assembling, supramolecular chemistry and pharmacology of amphotericin B: poly-aggregates, oligomers and monomers, J. Control. Release 341 (2022) 716–732, https://doi.org/10.1016/j.jconrel.2021.12.019.
[21] B. Wang, et al., Construction of high drug loading and enzymatic degradable multilayer films for self-defense drug release and long-term biofilm inhibition, Biomacromolecules 19 (2018) 85–93, https://doi.org/10.1021/acs.biomac.7b01268.
[22] M.-H. Xiong, et al., Bacteria-responsive multifunctional Nanogel for targeted antibiotic delivery, Adv. Mater. 24 (2012) 6175–6180, https://doi.org/10.1002/adma.201202847.
[23] D. Aouameur, et al., Stimuli-responsive gel-micelles with flexible modulation of drug release for maximized antitumor efficacy, Nano Res. 11 (2018) 4245–4264, https://doi.org/10.1007/s12274-018-2012-1.
[24] M. Wichert, et al., Dual-display of small molecules enables the discovery of ligand pairs and facilitates affinity maturation, Nat. Chem. 7 (2015) 241–249, https://doi.org/10.1038/nchem.2158.
[25] J. Vila, et al., Antibacterial evaluation of a collection of norfloxacin and ciprofloxacin derivatives against multiresistant bacteria, Int. J. Antimicrob. Agents 28 (2006) 19–24, https://doi.org/10.1016/j.ijantimicag.2006.02.013.
[26] W.A. Craig, Overview of newer antimicrobial formulations for overcoming pneumococcal resistance, Am. J. Med. Suppl. 117 (2004) 16–22, https://doi.org/10.1016/j.amjmed.2004.07.004.
[27] C. Wang, Q. Chen, Z. Wang, X. Zhang, An enzyme-responsive polymeric superamphiphile, Angew. Chem. 122 (2010) 8794–8797, https://doi.org/10.1002/ange.201004253.
[28] M. Shahriari, et al., Enzyme responsive drug delivery systems in cancer treatment, J. Control. Release 308 (2019) 172–189.
[29] T.M. Allen, Ligand-targeted therapeutics in anticancer therapy, Nat. Rev. Cancer 2 (2002) 750–763, https://doi.org/10.1038/nrc903.
[30] E. Turos, et al., Antibiotic-conjugated polyacrylate nanoparticles: new opportunities for development of anti-MRSA agents, Bioorg. Med. Chem. Lett. 17 (2007) 53–56, https://doi.org/10.1016/j.bmcl.2006.09.098.
[31] L. Pichavant, et al., Vancomycin functionalized nanoparticles for bactericidal biomaterial surfaces, Biomacromolecules 17 (2016) 1339–1346, https://doi.org/10.1021/acs.biomac.5b01727.
[32] E.F. Panarin, M.V. Solovskij, Polymer derivatives of β-lactam antibiotics of the penicillin series, J. Control. Release 10 (1989) 119–129, https://doi.org/10.1016/0168-3659(89)90023-0.
[33] M. Schmidt, et al., Poly(2-oxazoline)–antibiotic conjugates with Penicillins, Bioconjug. Chem. 28 (2017) 2440–2451, https://doi.org/10.1021/acs.bioconjchem.7b00424.
[34] M. Schmidt, et al., Conjugation of ciprofloxacin with poly(2-oxazoline)s and polyethylene glycol via end groups, Bioconjug. Chem. 26 (2015) 1950–1962, https://doi.org/10.1021/acs.bioconjchem.5b00393.
[35] M. Schmidt, et al., Insights into the kinetics of the resistance formation of Bacteria against ciprofloxacin poly(2-methyl-2-oxazoline) conjugates, Bioconjug. Chem. 29 (2018) 2671–2678, https://doi.org/10.1021/acs.bioconjchem.8b00361.
[36] A. Romanovska, et al., Conjugates of ciprofloxacin and amphiphilic block Copoly (2-alkyl-2-oxazolines) s overcome efflux pumps and are active against CIP-resistant Bacteria, Mol. Pharm. 18 (2021) 3532–3543, https://doi.org/10.1021/acs.molpharmaceut.1c00430.

[37] H.S. Abandansari, E. Aghaghafari, M.R. Nabid, H. Niknejad, Preparation of injectable and thermoresponsive hydrogel based on penta-block copolymer with improved sol stability and mechanical properties, Polymer 54 (2013) 1329–1340, https://doi.org/10.1016/j.polymer.2013.01.004.
[38] N.K. Singh, D.S. Lee, In situ gelling pH-and temperature-sensitive biodegradable block copolymer hydrogels for drug delivery, J. Control. Release 193 (2014) 214–227, https://doi.org/10.1016/j.jconrel.2014.04.056.
[39] M. Alami-Milani, et al., Novel pentablock copolymers as thermosensitive self-assembling micelles for ocular drug delivery, Adv. Pharm. Bull. 7 (2017) 11, https://doi.org/10.15171/apb.2017.003.
[40] A.P. Constantinou, K. Zhang, B. Somuncuoğlu, B. Feng, T.K. Georgiou, PEG-based methacrylate tetrablock terpolymers: how does the architecture control the gelation? Macromolecules 54 (2021) 6511–6524, https://doi.org/10.1021/acs.macromol.1c00349.
[41] A.H. Gröschel, et al., Guided hierarchical co-assembly of soft patchy nanoparticles, Nature 503 (2013) 247–251, https://doi.org/10.1038/nature12610.
[42] A. Steinhaus, et al., Controlling Janus nanodisc topology through ABC triblock terpolymer/homopolymer blending in 3D confinement, Macromolecules 54 (2021) 1224–1233, https://doi.org/10.1021/acs.macromol.0c02769.
[43] A.R. Rodriguez, U.-J. Choe, D.T. Kamei, T.J. Deming, Blending of diblock and triblock copolypeptide amphiphiles yields cell penetrating vesicles with low toxicity, Macromol. Biosci. 15 (2015) 90–97, https://doi.org/10.1002/mabi.201400348.
[44] M. Schmidt, et al., Investigations on “near perfect” poly(2-oxazoline) based amphiphilic polymer conetworks with a crystallizable block, Eur. Polym. J. 88 (2017) 562–574, https://doi.org/10.1016/j.eurpolymj.2016.09.046.
[45] S.A. Wilhelm, M. Maricanov, V. Brandt, F. Katzenberg, J.C. Tiller, Amphiphilic polymer conetworks with ideal and non-ideal swelling behavior demonstrated by small angle X-ray scattering, Polymer 242 (2022) 124582, https://doi.org/10.1016/j.polymer.2022.124582.
[46] K. Kempe, M. Lobert, R. Hoogenboom, U.S. Schubert, Screening the synthesis of 2-substituted-2-oxazolines, J. Comb. Chem. 11 (2009) 274–280, https://doi.org/10.1021/cc800174d.
[47] C.P. Fik, et al., Impact of functional satellite groups on the antimicrobial activity and hemocompatibility of telechelic poly(2-methyloxazoline)s, Biomacromolecules 13 (2012) 165–172, https://doi.org/10.1021/bm201403e.